Journal of Physics: Conference Series **135** (2008) 012051 doi:10.1088/1742-6596/135/1/012051

Identification of boiling heat fluxes in a single-bubble nucleate boiling experiment using a three-dimensional transient heat conduction model

Y Heng[1], A Mhamdi[1], E Wagner[2], P Stephan[2], W Marquardt[1]

[1]Aachener Verfahrenstechnik, Lehrstuhl für Prozesstechnik, RWTH Aachen University, Turmstr. 46, D-52064 Aachen, Germany

[2]Fachgebiet Technische Thermodynamik, TU Darmstadt, Petersenstr. 30, D-64287 Darmstadt, Germany

E-mail: yi.heng@avt.rwth-aachen.de, adel.mhamdi@avt.rwth-aachen.de, wagner@ttd.tu-darmstadt.de, pstephan@ttd.tu-darmstadt.de, wolfgang.marquardt@avt.rwth-aachen.de

Abstract. Boiling heat transfer is still hard to model and to predict. Among all kinds of studies on boiling processes, the estimation of the local heat fluxes on the boiling surface is fundamental. From the mathematical point of view, it belongs to the class of inverse heat conduction problems (IHCPs) which cannot be solved straightforwardly. In this paper, we estimate the local boiling heat flux by solving a three-dimensional (3D) transient IHCP using the measured temperature field from a single-bubble nucleate boiling experiment. The considered IHCP is formulated as a mathematical optimization problem and solved by the conjugate gradient (CG) method.

1. Introduction

Although many investigations of boiling phenomena have been conducted during the past decades, boiling heat transfer is still not fully understood. Boiling heat flux has been considered to be correlated with many different parameters, e.g. superheat, nucleate site density or bubble diameter in the nucleate boiling and average vapor fraction or vapor velocity in transition boiling [1]. Dhir and Liaw [2] have developed a unifying framework for nucleate and transition boiling on base of a macroscopic geometry model of "vapor stems". On the mesoscale, single bubbles growing on a heated plate or emerging out of the closed film in film boiling have been studied in detail [3, 4, 5]. On the microscale, the microlayer theory proposed by Stephan and Hammer [6] predicts that most of the heat during boiling is transferred in the micro-region of the three-phase contact line by evaporation. Most of the existing approaches have not been fully validated yet because of the lacking of experimental and theoretical evidence. It is not completely clear yet which parameters dominate boiling heat transfer. An adequate understanding of the various physical effects can only be obtained if high resolution measurement techniques and corresponding data processing methods are employed.

In this paper, we consider boiling experiments at a single artificial nucleation site which have been conducted at TU Darmstadt [7]. As shown in Fig. 1(a), single bubbles are generated on top of a metallic foil heater (1), which is mounted onto a copper plate (3) with a circular

opening (4) in the middle. The plate is fixed onto a base plate (5). Electrodes (2) are enclosed in an insolating frame (9) and pressed from both sides with grub screws (10) against the foil to guarantee a good electric contact. Through the opening (4) and an IR transparent substrate (6) the bottom side of the heating foil is optically accessible. Since in this experiment nucleate boiling must be avoided at any potential sites other than the artificial one in the center of the foil, the entire outer assembly is cooled down some degrees below saturation temperature using coolant bores (11) in the base plate (5). Ports for coolant (12) and electric current (8) are placed at the bottom side. Different types of artificial nucleation sites were examined. The experimental results in [7] were carried out on a 50 μm thick stainless steel foil with a bore whole of about 25 μm diameter. A scanning electron microscope (SEM) picture of the nucleation site is shown in Fig. 1(b). The temperature field at the back side of the heater was observed with a high-speed infrared camera. The total measurement uncertainty of the IR sensor is about 0.5 K. At a resolution of 152×144 pixels, a frame rate of 987 Hz could be applied. The resulting pixel size conforms to a square of 16×16 microns.

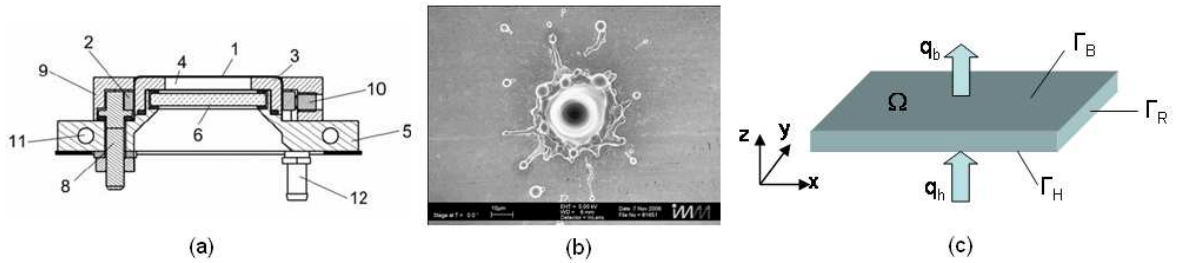

Figure 1. (a) Cross sectional view of the foil heater (adopted from [7]), (b) Nucleation site produced by laser beam at IMM (adopted from [7]), (c) Schematic representation of the 3D heating foil.

In [7], the local boiling heat flux was computed using a two-dimensional (2D) heat conduction model together with a filter-based inversion algorithm. In this work, we consider the estimation of the local heat flux at the boiling surface using the solution approach presented in [8], where the spatial domain is modelled in 3D. A 3D domain is chosen because the origin of the signal is an event of about 1 μm lateral extension with an amplitude of 10^6 W/m^2. Thus, a vertical temperature gradient (in z-direction) can not be neglected. Estimation of the heat flux on the boiling boundary from a measured temperature field on the back of the thin heater belongs to the class of IHCPs [9], which are ill-posed in the sense of Hadamard [10]. In particular, the stability condition is violated. Namely, small perturbation in the data leads to large deviations of estimated quantities. Regularization strategies are often applied to obtain useful solutions for IHCPs [11, 12].

In Section 2, we first give the mathematical formulation for the IHCP considered. An optimization-based solution method is then presented in Section 3. To validate and assess the performance of the solution method, a simulation case study is presented in Section 4. In Section 5, we show the estimation results with real measurement data from [7]. Conclusions and an outlook will be given in the final section.

2. The inverse heat conduction problem

We consider the 3D domain Ω shown in Fig. 1(c) with boundary $\partial\Omega = \Gamma_H \cup \Gamma_B \cup \Gamma_R$, where Γ_H, Γ_B and Γ_R denote the heated, the boiling and the adiabatic boundaries of Ω, respectively. The linear heat conduction problem for the temperature $T(\mathbf{x}, t)$ is given by

$$\frac{\partial T(\mathbf{x},t)}{\partial t} = a\Delta T(\mathbf{x},t), \quad (\mathbf{x},t)\in\Omega\times[0,t_f], \tag{1}$$
$$T(\mathbf{x},0) = T_0(\mathbf{x}), \quad \mathbf{x}\in\Omega, \tag{2}$$
$$-\lambda\frac{\partial T(\mathbf{x},t)}{\partial n} = q_h(\mathbf{x},t), \quad (\mathbf{x},t)\in\Gamma_H\times[0,t_f], \tag{3}$$
$$-\lambda\frac{\partial T(\mathbf{x},t)}{\partial n} = q_b(\mathbf{x},t), \quad (\mathbf{x},t)\in\Gamma_B\times[0,t_f], \tag{4}$$
$$-\lambda\frac{\partial T(\mathbf{x},t)}{\partial n} = 0, \quad (\mathbf{x},t)\in\Gamma_R\times[0,t_f], \tag{5}$$

where λ and a are the known constant thermal conductivity and diffusivity coefficients. T_0, q_h and q_b are the initial and boundary conditions, respectively. The final time is denoted by t_f and the outer normal on the boundaries is denoted by n.

The considered *inverse heat conduction problem* corresponds to the estimation of the unknown heat flux q_b at the boiling surface Γ_B from the measured temperature field T_m on the back of the thin heater Γ_H given the model governed by eqs. (1)–(5).

3. The solution method

The solution of the inverse problem is obtained from minimizing the objective functional

$$J(q_b) := \int_0^{t_f}\int_{\Gamma_H}[T(\mathbf{x},t;q_b) - T_m(\mathbf{x},t)]^2 d\mathbf{x}dt, \tag{6}$$

where $T(\mathbf{x},t;q_b)$ denotes temperatures determined from the solution of problem (1)–(5) for a certain q_b.

The CG method is used to solve the optimization problem (6) by setting up an iteration sequence for the unknown function $q_b(\mathbf{x},t)$ [8, 13]. An estimate $\hat{q_b}^{k+1}$ of q_b at iteration k is computed from

$$\hat{q_b}^{k+1}(\mathbf{x},t) = \hat{q_b}^{k}(\mathbf{x},t) - \mu^k P^k(\mathbf{x},t), \text{ for } k = 0,1,2,... \tag{7}$$

We choose $\hat{q_b}^0 = 0$, $P^0 = \nabla J^0$ as initial guesses. $P^k(\mathbf{x},t)$ is the conjugate search direction which is updated at each iteration by

$$P^k(\mathbf{x},t) = \nabla J^k(\mathbf{x},t) + \gamma^k P^{k-1}(\mathbf{x},t), \tag{8}$$

where the conjugate coefficient γ^k is determined from

$$\gamma^k = \frac{\int_0^{t_f}\int_{\Gamma_B}[\nabla J^k]^2 d\mathbf{x}dt}{\int_0^{t_f}\int_{\Gamma_B}[\nabla J^{k-1}]^2 d\mathbf{x}dt}. \tag{9}$$

Thus, at each iteration step, we need to evaluate the gradient ∇J^k and the search step length μ^k. The gradient is obtained from

$$\nabla J^k(\mathbf{x},t)|_{\Gamma_B} = [-\frac{a}{\lambda}\cdot\psi(\mathbf{x},t)]_{|\Gamma_B}, \tag{10}$$

where the adjoint variable ψ satisfies the adjoint equations

$$\frac{\partial \psi(\mathbf{x},t)}{\partial t} = -a\Delta\psi(\mathbf{x},t), \quad (\mathbf{x},t)\in\Omega\times[0,t_f], \tag{11}$$
$$\psi(\mathbf{x},t_f) = 0, \quad \mathbf{x}\in\Omega, \tag{12}$$
$$-\lambda\frac{\partial \psi(\mathbf{x},t)}{\partial n} = 2[T(\mathbf{x},t;\hat{q_b}^k) - T_m(\mathbf{x},t)], \quad (\mathbf{x},t)\in\Gamma_H\times[0,t_f], \tag{13}$$
$$-\lambda\frac{\partial \psi(\mathbf{x},t)}{\partial n} = 0, \quad (\mathbf{x},t)\in\Gamma_B\cup\Gamma_R\times[0,t_f]. \tag{14}$$

The search step length μ^k is computed by

$$\mu^k = \frac{\int_0^{t_f}\int_{\Gamma_H}[T(\mathbf{x},t;\hat{q_b}^k) - T_m(\mathbf{x},t)]S(\mathbf{x},t)d\mathbf{x}dt}{\int_0^{t_f}\int_{\Gamma_H}[S(\mathbf{x},t)]^2 d\mathbf{x}dt}, \tag{15}$$

where S is obtained from the following sensitivity equations

$$\frac{\partial S(\mathbf{x},t)}{\partial t} = a\Delta S(\mathbf{x},t), \quad (\mathbf{x},t) \in \Omega \times [0,t_f], \tag{16}$$

$$S(\mathbf{x},0) = 0, \quad \mathbf{x} \in \Omega, \tag{17}$$

$$-\lambda\frac{\partial S}{\partial n}(\mathbf{x},t) = P^k(\mathbf{x},t), \quad (\mathbf{x},t) \in \Gamma_B \times [0,t_f], \tag{18}$$

$$-\lambda\frac{\partial S}{\partial n}(\mathbf{x},t) = 0, \quad (\mathbf{x},t) \in \Gamma_H \cup \Gamma_R \times [0,t_f]. \tag{19}$$

The problem (11)–(14) is a final-time value problem. By introducing a new time variable $t' = t_f - t$, it can be transformed to a standard initial value problem. The arising *direct*, *adjoint* and *sensitivity* partial differential equations (PDEs) in each optimization iteration are solved using the software package DROPS [14].

4. Simulation case study

In this section, a simulation case study involving a ring-shaped boiling heat flux is set up. We consider the 3D domain $\Omega := 1 \times 1 \times 0.05$ mm^3. The material properties are chosen the same as those of the heating foil used in the experiment [7], where the density $\rho = 7900$ kg/m^3, specific heat $c = 520$ J/kgK and thermal conductivity $\lambda = 14.5$ W/mK result in a thermal diffusivity of $a = 3.53 \times 10^{-6}$ m^2/s. The initial and known boundary conditions are $T_0 = 55°C$ and $q_h = 5000$ W/m^2, respectively. The simulation time interval is $0 \le t \le 0.05$ s. A one-step implicit Euler scheme with a step size $\tau = 0.001$ s is used for time discretization.

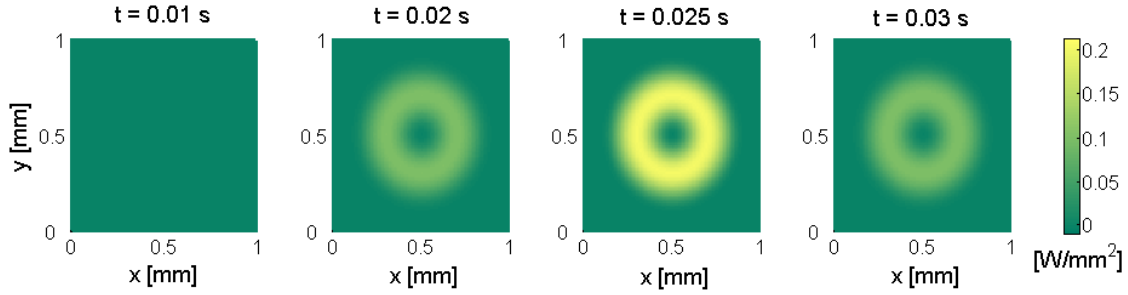

Figure 2. The exact heat flux q_b^{ex} at different time instants.

The exact heat flux (in W/mm^2) is defined as $q_b^{ex}(x,y,t) = \alpha(t) \cdot \beta(x,y), \quad (x,y,t) \in \Gamma_B \times [0,0.05]$, where $\alpha(t) = 0.1sin(100\pi(t-0.02))+0.1$ for $0.015 \le t \le 0.035$, zero otherwise, and $\beta(x,y) = 0.5sin(5\pi(0.3 - \sqrt{(x-0.5)^2+(y-0.5)^2})) + 0.5$ for $\sqrt{(x-0.5)^2+(y-0.5)^2} \le 0.4$, zero otherwise. Fig. 2 shows this heat flux function at some time instants.

A uniform space discretization with piece-wise linear finite elements on a tetrahedral grid is employed. 101×101 unknowns in the x–y-plane and only six unknowns in the z-direction are used. After investigating the effect of the discretization in the z-direction for six and more unknowns on the temperature profile, only negligible differences have been observed. Hence, we

conclude that such a coarse grid is already appropriate for the resolution of the temperature changes in z-direction.

The exact temperature T_m^{ex} is computed from the solution of the direct problem with known q_b^{ex} on Γ_B. The perturbed data are constructed by adding an artificial measurement error ω to T_m^{ex}. The perturbed measurement T_m is given by $T_m = T_m^{ex} + \sigma\omega$, where σ is the standard deviation of the measurement error. ω is generated from a zero mean normal distribution with variance one. Here we choose a measurement error of approximately 10%, which corresponds to $\sigma = 0.115$.

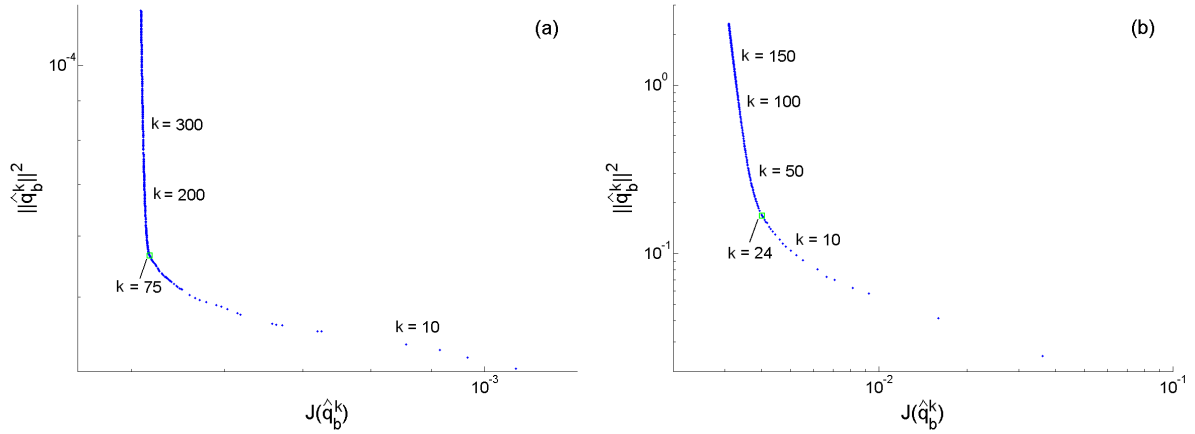

Figure 3. (a) L-curve for estimation with perturbed measurements with error level $\sigma = 0.115$, (b) L-curve for the experimental data.

Due to the ill-posedness of the considered IHCP, the estimation quality will decrease if too many optimization iterations are applied, whereas the residual is getting smaller. Here we apply the L-curve criterion [15, 16] to find the best termination index. The L-curve shown in Fig. 3(a) is a parameterized plot of the residual (6) against the solution norm

$$||\hat{q}_b{}^k||^2 := \int_0^{t_f} \int_{\Gamma_B} [\hat{q}_b{}^k(\mathbf{x}, t)]^2 d\mathbf{x}dt. \tag{20}$$

The best termination index is found at the maximum curvature of L-curve.

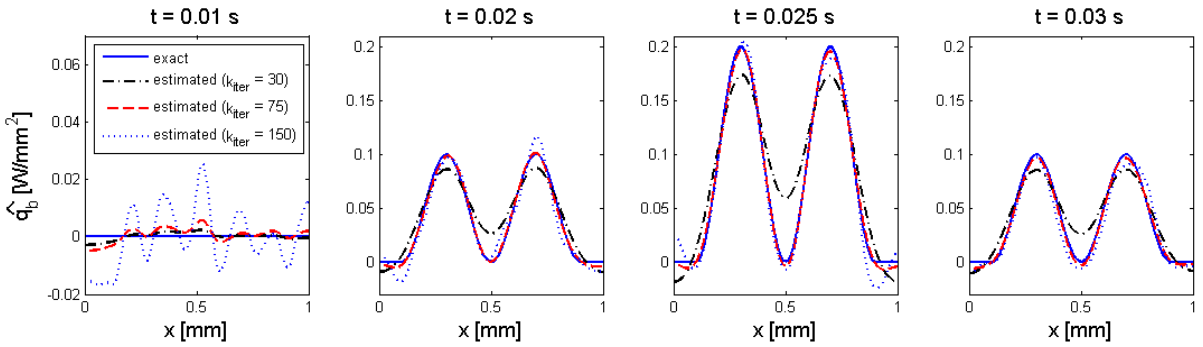

Figure 4. Temporal evolution of estimated heat fluxes along the 2D line with $y = 0.5$ mm for different numbers of optimization iterations k_{iter}.

Since q_b^{ex} is symmetric in space (see Fig. 2), it is sufficient to show the estimation results along the 2D line where $y = 0.5$ mm. From the estimation results shown in Fig. 4, we observe for a low number of CG iterations, e.g. $k_{iter} = 30$, the local extrema of the estimated heat fluxes have not yet been well-estimated. Before the best termination index, the overall estimation quality is improving as the number of optimization iterations increases. The estimated heat flux for the best termination index, $k_{iter} = 75$, is very close to the exact one. For higher iterations, the estimated heat flux quickly starts to oscillate and not any more approaches the exact one. This phenomenon can be observed by the estimation results obtained for $k_{iter} = 150$ (see Fig. 4). Such effect is due to the ill-posedness of the considered IHCP.

5. Estimation results with experimental data

In the considered experiment [7], the thin heater has a thickness of 50 μm and the measurement section has a spatial resolution of 152×144 pixel with a pixel size of 16×16 μm. We define the 3D computational domain $\Omega := 2.416 \times 2.288 \times 0.05$ mm^3. The space discretization of the model considers the same resolution as the measurement data. This results in 152×144 unknowns in the x–y-plane. Based on the investigation in the simulation case study, we use six unknowns for the space discretization in z-direction. 50 time frames of temperature measurements are taken with a sampling frequency of 987 Hz. This translates to a time step size of $\tau \approx 1.013$ ms for the time discretization.

The initial temperature distribution T_0 is assumed to be constant across the foil thickness. A calculated input heat flux $q_h = 5356$ W/m^2 is applied. The measurement was conducted with a constant heating current of 12.36 A. Since there is an unknown voltage drop at the electrodes, the heat flux was calculated using the electric resistance of the heating foil with $\rho = 0.7$ Ohm·mm/m for the first estimations. It has to be mentioned that for more quantitative interpretations, the temperature coefficient must be taken into account. The material properties have already been mentioned in the simulation case study.

The measured temperature distribution (in K) on the x–y-plane at time frames 23-30 is depicted in Fig. 5 which correspond to a single bubble cycle, as confirmed by simultaneous imaging with a high speed camera. The noise of the scanner is 0.13 K (95% of the values are in this range). The signal has an amplitude of about 1.5 K. Thus, the signal to noise ratio is around 11.5. A cold region in the temperature distribution at frame 23 is the result of the activity of an earlier bubble. Frames 24-30 correspond to the period where the new bubble grows and starts to depart from the contact surface. We see that the size of the cold spot first increases in magnitude at frames 24-27 (bubble grows) and then has little change at frames 28-30 (bubble starts to depart from the surface).

The best estimated surface boiling heat fluxes (in W/m^2) are shown in Fig. 6. The estimations are obtained after $k_{iter} = 24$ CG iterations, determined from the maximum curvature point of the L-curve (see Fig. 3(b)). From these estimation results, it is apparent that the boiling heat flux undergoes a significant change during the single bubble cycle and a ring-shaped region of the local heat flux is observed. The peak value of the estimated heat fluxes is nearly 30 times larger than their average value. These estimation results confirm those obtained in [7], which were computed using an approximate 2D heat conduction model. This may be explained by the small thickness of the heating foil.

Near the surface boundary and in the center of boiling surface at time frames 29-30, we observe an estimate of negative heat fluxes. This result may be explained in different ways. The negative heat flux estimates might be an artefact of the numerical computation, which results from the fact that the presented solution method intends to yield a smooth approximation for the unknown boiling heat flux. In case that the unknown heat flux function is non-smooth, non-differentiable or even non-continuous at some temporal and spatial positions, small oscillated estimates around these positions will appear and this may lead to negative estimated heat fluxes.

Alternatively, because the heat flux calculation is also sensitive to the electric heat input, an underestimated input heat flux q_h may lead to negative estimated boiling heat fluxes. Thus, for more reliable interpretation, the error of the heat flux calculation should be included.

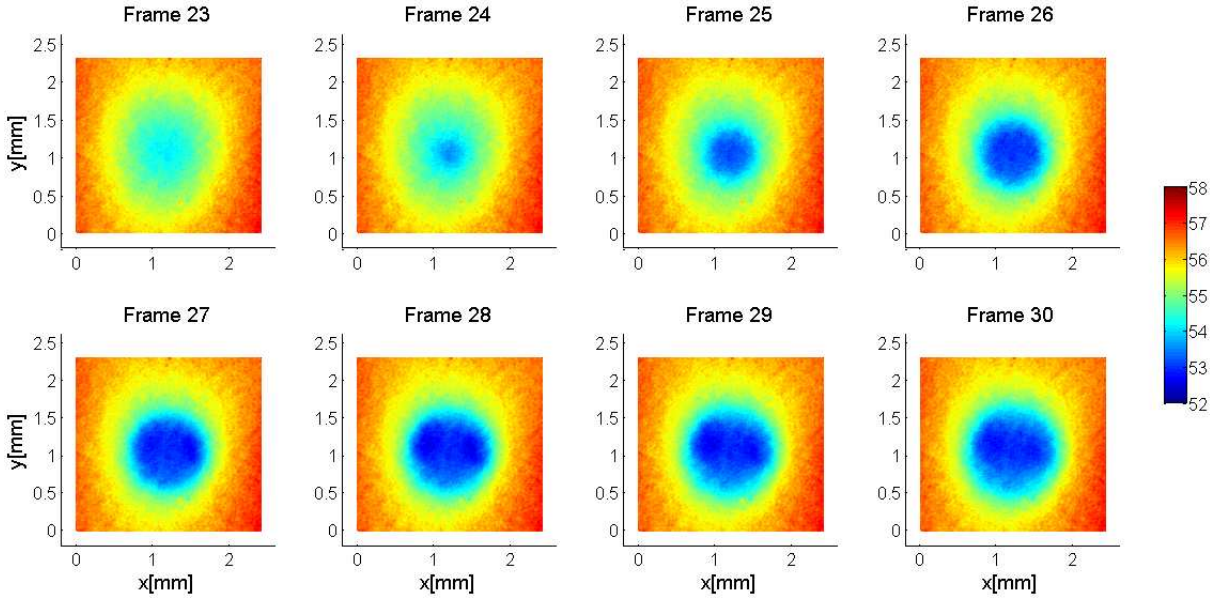

Figure 5. The measured temperature field on the back side of the heater

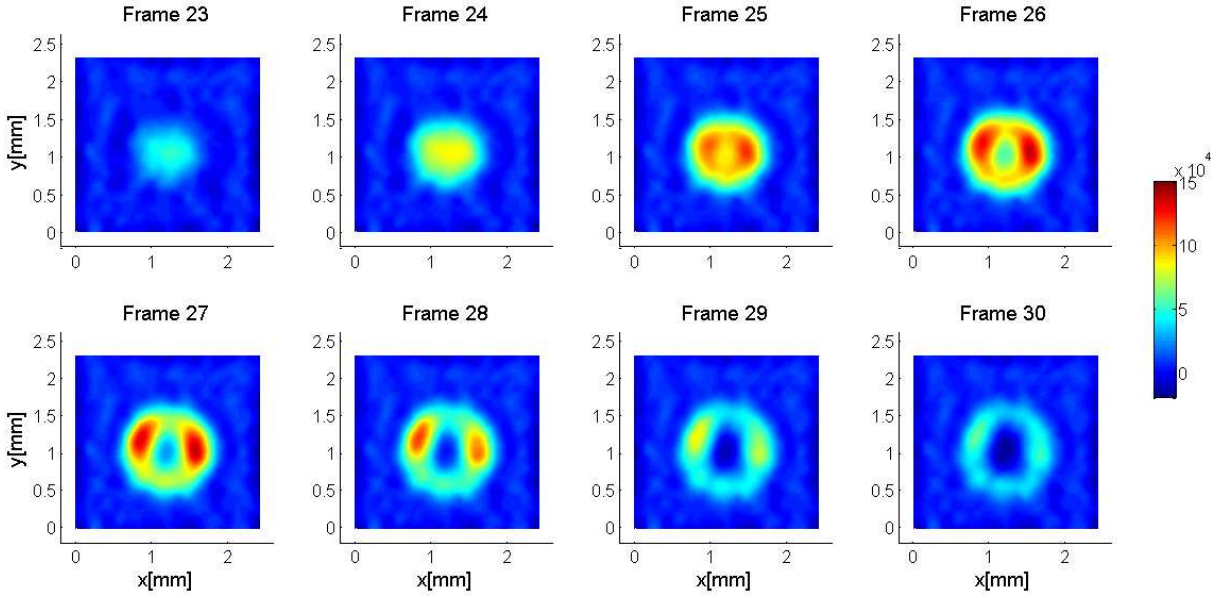

Figure 6. The best estimated surface boiling heat flux at time frames 23-30.

6. Conclusions

We have successfully applied an optimization-based solution approach to estimate the local boiling heat flux in a single-bubble nucleate boiling experiment from the high resolution

measured temperature field taken on the back side of the thin heater. The presented estimation results are computed on a spatially and temporally discretized model with high resolution. Altogether $152 \times 144 \times 50 = 1094400$ spatial and temporal parameters have been used to estimate the unknown boiling heat flux function. From the estimation results, we have observed that the boiling heat flux in most of the surface region undergoes little change. Although the computation cost using the finely discretized model is acceptable, the large number of parameters used for estimation which undergo little change are redundant. Future work will be devoted to reduce the number of parameters by applying a solution strategy which adaptively discretizes the computation domain during the estimation process. Reducing the number of estimation parameters is expected to not only improve the computation efficiency, but also contribute to a better regularization of the estimated quantities. Besides, since the input heat flux q_h is also crucial for the estimation of unknown boiling heat flux q_b, a sensitivity study to the calculation errors on q_h will be performed in order to evaluate the error on q_b.

Acknowledgments

The authors gratefully acknowledge the financial support by German Science Foundation (DFG) through the research training group GRK 775 and a joint research project on fundamentals of boiling heat transfer within the boiling package "Sieden binärer Gemische".

References

[1] Carey V P 1992 *Liquid-Vapor Phase-Change Phenomena* (New York: Hemisphere Publishing Corporation)
[2] Dhir V K and Liaw S P 1989 *J. Heat Transfer* **111(3)** 739-746
[3] Dhir V K 2001 *AlChE J.* **47(4)** 813-834
[4] Mei R, Chen W and Klausner J F 1995 *Int. J. Heat Mass Transfer* **38(5)** 909-919
[5] Mei R, Chen W and Klausner J F 1995 *Int. J. Heat Mass Transfer* **38(5)** 921-934
[6] Stephan P and Hammer J 1994 *Wärme- und Stoffübertragung* **30** 119-125
[7] Wagner E *et al* 2007 6^{th} *Int. Conf. on Multiphase Flow (Leipzig)*
[8] Groß S, Soemers M, Mhamdi A, Al Sibai F, Reusken A, Marquardt W and Renz U 2005 *Int. J. Heat Mass Transfer* **48** 5549-5562
[9] Alifanov O M 1994 *Inverse Heat Transfer Problems* (Berlin: Springer)
[10] Hadamard J 1923 *Lectures on Cauchy's Problem in Linear Partial Differential Equations* (New Haven: Yale University Press)
[11] Beck J *et al* 1985 *Inverse Heat Conduction. Ill-Posed Problems* (New York: Wiley)
[12] Tikhonov A N *et al* 1977 *Solutions of Ill-posed Problems* (Washington: V. H. Winston and Sons)
[13] Huang C H and Wang S P 1999 *Int. J. Heat Mass Transfer* **42** 3387-3403
[14] Groß S *et al* 2002 *The DROPS Package for Numerical Simulations of Incompressible Flows Using Parallel Adaptive Multigrid Techniques* (Aachen: Technical Report No. 211, IGPM)
[15] Hansen P C 1998 *Rank-Deficient and Discrete Ill-posed Problems: Numerical Aspects of Linear Inversion* (Philadelphia: SIAM)
[16] Engl H W *et al* 1996 *Regularization of Inverse Problems* (Dordrecht: Kluwer Academic Publishers)